Multi-site surface complexation modelling of Se(IV) sorption on biotite

Xiaodong Li[a,*], Eini Puhakka[a], Longcheng Liu[b], Wenzhong Zhang[a], Jussi Ikonen[a], Antero Lindberg[c], Marja Siitari-Kauppi[a]

[a] Department of Chemistry-Radiochemistry, University of Helsinki, P.O. Box 55, FI-00014, Finland
[b] Department of Chemical Engineering, KTH Royal Institute of Technology, S-10044 Stockholm, Sweden
[c] Geological Survey of Finland, Betonimiehenkuja 4, FI-02151 Espoo, Finland

ARTICLE INFO

ABSTRACT

A surface complexation model of Se(IV) sorption on biotite with one type of strong sorption sites and two types of weak sorption sites were developed based on experimental data obtained from titration, sorption edge and sorption isotherm experiments. Titration data was collected using a batch-wise manner together with back-titration to calibrate the effect of mineral dissolution in 0.01 M KClO$_4$ background electrolytes from pH 3 to 11 in an inert atmosphere glovebox. Further calibrations of the titration curve include proton exchange and cation exchange in which the calculations of cation occupancies on biotite surfaces were taken into account. The sorption edge measurements were determined by measuring the sorption of 10^{-9} M total Se with a radioactive Se-75 tracer on converted biotite in 0.01 M KClO$_4$ solution from pH 3 to 11. Se sorption was observed to be strongly dependent on pH. Surface complexation modelling was performed by deriving a set of optimized parameters that can fit titration, sorption edge and sorption isotherm (at pH ~7.7) experimental data. A CASTEP code implemented into Materials Studio was used to calculate the site densities and site types on the biotite surfaces. Weak sorption sites with site densities of 3.2 sites/nm^2 and 1.4 sites/nm^2 were derived from the codes and used in the sorption model. A computer code that coupled PHREEQC with Python was developed for the fitting and optimizing processes. The model was validated by sorption data at pH ~9.5. The results show that the model can provide quantitative predicts of Se(IV) sorption in groundwater conditions of a deep geological repository and help improve the performance assessments by giving more convincing estimates of the release of radionuclides towards aquifers and biosphere.

1. Introduction

The main objective of the disposal of spent nuclear fuel is to guarantee long-term isolation of the waste from biosphere and surface environment (De Cannière et al., 2010; Ewing, 2015; Posiva Oy, 2013; SKB, 1999a, 1999b; Söderlund, 2016). In many countries, the deep geological repository consists of crystalline rocks like granite or granodiorite as a host rock, which is the final natural barrier providing retention for radionuclides presented in the spent nuclear fuel (Kitamura et al., 1999; Muuri et al., 2016; Soler et al., 2015; Soler and Mäder, 2007; Tsai et al., 2009). To evaluate the safety of a nuclear waste repository, performance assessment is carried out to ensure that humans and the environment are sufficiently protected from harmful effects of radiation. This is conducted by evaluating quantitatively the transport of potentially released radionuclides through engineered and geologic barriers and the consequences for humans and the environment in biosphere. (Altmann, 2008; Mahmoudzadeh et al., 2014; Meng et al.,

2018; Missana et al., 2008; Shahkarami et al., 2016; Widestrand et al., 2010). Se-79, one of the fission products from spent nuclear fuel, is a critical radionuclide for long-term safety of a nuclear waste repository due to its long half-life (3.7×10^5 years) and high mobility (De Cannière et al., 2010; Ervanne et al., 2016; Ewing, 2015; Ikonen et al., 2016b; Kim et al., 2012; Söderlund et al., 2016b). It has a high impact on the cumulative radiation dose in a spent nuclear fuel repository and needs great concern for the safety assessments (Atwood, 2010; Lehto and Hou, 2011).

To evaluate the retardation processes of Se under conditions expected in underground repositories during performance assessment, the sorption distribution coefficient (K_d) found from the sorption database is commonly used. Many researchers have studied and given their K_d values for Se based on batch sorption experiments with different crushed minerals (Ikonen et al., 2016a, 2016b) or from in-situ experiments (Jokelainen et al., 2013; Vilks et al., 2003; Widestrand et al., 2007, 2010). However, to give more detailed analysis of the sorption

processes, the development of a sorption model is necessary (Ervanne et al., 2013, 2016; Ikonen et al., 2016b; Missana et al., 2009; Puhakka and Olin, 2014; Söderlund et al., 2016b). A sorption model can supply information of the sorption mechanisms of a radionuclide and help understand the sorption processes deeply. In addition, quantitative predictions of the sorption results under different geochemical conditions are only feasible with the aid of a validated sorption model. Since the geological conditions in a nuclear waste repository evolve with the surroundings over time, a model that can provide results with future environmental changes is more valuable than sorption K_d values that were obtained with specific conditions in laboratories.

However, only a few studies investigated the sorption problem with a mechanistic approach. Missana et al. (2009) studied the sorption of selenite onto illite and smectite clays experimentally and provided a one-site model to fit the sorption data from pH 4 to 8, though some of the modelling parameters were directly taken from other literatures. Bradbury and Baeyens presented a batch titration method to measure the pKs of protonation and deprotonation reactions of sorption sites on surfaces of illite and montmorillonite. Based on the titration results, a 2-site protolysis non-electrostatic surface complexation and cation exchange (2SPNE SC/CE) sorption model was successfully developed to describe the uptake of radionuclides on these two clay minerals (Baeyens and Bradbury, 1995a; Bradbury and Baeyens, 2005a, 2009a). However, quite few studies exist concerning Se sorption onto biotite mineral with a mechanistic modelling method.

Researchers have shown that biotite has much larger specific surface area (SSA) than the other main minerals of granite and granodiorite (Li et al., 2018) and the Se sorption on biotite can, basically, represent its sorption on the whole bedrock (Yang et al., 2018). Thus, the aim of this work was to develop a multi-site surface complexation model for Se(IV) sorption onto biotite based on experimental data from titration and sorption experiments. A batch forward titration combined with backtitration method was used to overcome the problem of mineral dissolution in order to measure the pKs of protonation and deprotonation reactions of sorption sites on surfaces of biotite. Molecular modelling was used to obtain some basic modelling parameters, such as site densities and site types. The technique of PHREEQC coupling with Python was used to calculate and optimize the fitting processes.

2. Materials and methods

2.1. Materials

The biotite used in this work was provided by the Geological Survey of Finland. The mineral was crushed by milling and the part with particle sizes 0.075 mm - 0.3 mm was used for titration and sorption experiments.

Commercial analytical grade $KClO_4$ was used after further recrystallization to minimize the effect of impurities on biotite sorption sites (Armarego and Chai, 2013).

Both stable (99%, Sigma-Aldrich) and radioactive selenium (Se-75) used in the experiments were in +IV oxidation state, in Na_2SeO_3 and $Na_2^{75}SeO_3$ form, respectively. Throughout the experimental procedures, both selenium forms remained in +IV oxidation state, which was studied by the HPLC-ICP-MS method (Li et al., 2018; Söderlund et al., 2016a, 2016b; Söderlund, 2016). The radioactive Se-75 was purchased from the Czech Metrology Institute with gamma impurities < 0.1%.

2.2. Mineral characterization

The characterization of biotite by X-ray diffraction (XRD), specific surface area (SSA) and cation exchange capacity (CEC) has been previously reported (Li et al., 2018). The XRD data showed that biotite was 100% (± 5%) pure phlogopite and the structural formula is given as $(KMg_{1.76}Fe_{0.7}Ti_{0.54})(Al_{1.08}Si_{2.92}O_{10})(OH_{0.44}F_{0.56}O)$.

The SSA and CEC data were determined to be 1.0323 ± 0.0041 m^2/g and 12.64 ± 0.42 meq/kg, respectively.

2.3. Preparation of crushed biotite samples for titration experiments

Impurities, such as Ca^{2+} and Na^+ that might be attached on the biotite surfaces, will cause errors in titration and cation/proton exchange experiments. Thus, a purifying procedure was applied to the crushed biotite sample to convert them into a mono-potassium form containing only K^+ at the exchange sites as far as possible. A cation exchange column was used for this conversion work. Ten grams of the crushed biotite sample was packed into a glass column, and 0.1 M $KClO_4$ and 0.01 M $KClO_4$ solutions were pumped through the column with a peristaltic pump at a flow rate of 4 mL/h. The equilibrium time was about one month to ensure that the accessible sorption sites were in the desired potassium form. The effluent samples were analyzed by Microwave Plasma – Atomic Emission Spectrometer (MP-AES 4200, Agilent). The conversion procedure ended when the concentrations of Mg^{2+}, Ca^{2+}, and Al^{3+} ions were under detection limits (< 0.01 ppm) and the concentration of Na^+ was 0.06 ppm.

2.4. Titration measurements

All the experiments were performed in an inert N_2 atmosphere glovebox with the concentration of CO_2 being about 10 ppm, and the concentration of O_2 being < 1 ppm.

Titration was carried out in a batch-wise manner and standard 0.1 M HCl and NaOH solutions of analytical reagent level were used. At first, 0.5 g converted biotite was equilibrated with 25 mL of 0.01 M $KClO_4$ while stirred in a 50 mL Sorvall polypropylene centrifuge tube for 3 days. Aliquots of standard acid or base were added to the pre-equilibrated biotite suspensions to give a series of initial pH between 3 and 11. Then the centrifuge tubes were shaken end-over-end for 24 h. Additional acid or base solutions were added into the centrifuge tubes to get the final wanted pH. After shaking, the tightly closed centrifuge tubes were transferred out of the glovebox and centrifuged followed by returning into the glovebox for sampling. Two samples were made from each single vial for different measurement purposes. Firstly, 5 mL of supernatant was taken from each vial and the pH were measured, after which the concentrations of Na, K, Ca, Mg, Al, Mn and Si were determined by MP-AES. Secondly, 15 mL of the supernatant was sampled for the subsequent backtitration. The backtitration was carried out by adding aliquots of standard base or acid solutions to each sample until the pH value was returned to the initial pH 7. The samples were stirred constantly and the time intervals of adding each aliquot of base or acid standard solution were > 5 min to achieve complete backtitration reactions.

2.5. Cation exchange selective coefficients measurements

Solutions containing $MgCl_2$, $CaCl_2$, $AlCl_3$ and $NaClO_4$ were used for checking the selective coefficients of cation exchange reactions between corresponding cations and K^+ ions on the biotite surface. Firstly, 0.5 g converted biotite and 25 mL of 0.01 M $KClO_4$ solution were left in a 50 mL polypropylene centrifuge tube to stabilize for 5 days to obtain equilibrium. Then, a series of samples with cation concentrations from 5×10^{-6} M to 1×10^{-3} M were prepared by adding 0.5 mL mother solution which contains different concentrations of corresponding cations. The sample vials were then shaken for one week, after which the samples were centrifuged. The pH of the supernatant was checked and the concentrations of different cations (K^+, Mg^{2+}, Ca^{2+}, Al^{3+}, Na^+) were measured by MP-AES.

2.6. Sorption of Se as a function of pH (Sorption edge) measurements

Sorption edge measurements were carried out with trace radioactive Se-75 concentration in a controlled N_2 atmosphere glovebox as shown

in Section 2.4. The aim was to obtain sorption capacity of selenium at 10^{-9} M (radiotracer added was 528 Bq/10 mL, corresponding 1.66×10^{-10} M) as a function of pH at fixed ionic strength. Firstly, 0.5 g converted biotite was first equilibrated with 25 mL of 0.01 M KClO$_4$ solution in a 50 mL polypropylene centrifuge tube for 3 days. Aliquots of standard acid or base were added to the vials together with proper amount of Se-75 and concentrated selenium solution in a way that the concentration of total selenium was 10^{-9} M in a pH series. The vials were then closed tightly and shaken end-over-end for 7 days. Subsequently they were transferred out of the glovebox and centrifuged. After returning to the glovebox, the pH of the supernatant was checked and sampled for radioactive measurement. Radioactive Se-75 was measured by a Hidex-AMG gamma counter in 8 mL background solutions. The measurement window covers the energies of the main gamma emissions of Se-75 (121 keV, 17.20%; 136 keV, 58.5%; 265 keV, 58.9%; 280 keV, 25.02%). The counting time was set to be 30 min.

2.7. Sorption as a function of concentration (sorption isotherm) measurements

The details of sorption isotherm measurement procedures have already been described in the previous publication (Li et al., 2018). Sorption isotherm measurements were performed to obtain the sorption data of Se(IV) on biotite sample with Se(IV) concentrations between 1.66×10^{-10} M to 1×10^{-3} M. The batch sorption experiments were conducted in two different ways. After stabilizing the mixture of biotite and 0.01 M KClO$_4$ for two weeks, in one way, non-radioactive selenium was added into the vials, causing a series of selenium concentration from 1×10^{-7} M to 1×10^{-3} M; in the other way, radioactive Se-75 mixed with non-radioactive selenium was added, and the total selenium concentration in the background solution was ranged from 1×10^{-10} M to 1×10^{-7} M. Then, all the vials were agitated for two weeks followed by centrifuging and sampling. For stable selenium, the concentration was determined with ICP-MS (Agilent 7500ce) while Hidex-AMG gamma counter was used to detect the Se-75 concentration.

The distribution coefficient K_d of selenium can be determined as follows,

$$K_d = \frac{C_0 - C_{aq}}{C_{aq}} \times \frac{V}{m}$$

where C_0 (mol/L) is the initial concentration of stable selenium in the solution or the selenium concentration derived from the activity of Se-75 in blank samples (without rock minerals). C_{aq} (mol/L) is the final concentration of stable selenium in the groundwater simulant or the selenium concentration that was derived from the activity of Se-75. V (L) is the volume of solution and m (Kg) the mass of the solid phase.

2.8. Modelling methods

The main purpose of the modelling is to find a set of parameters that could fit all the experimental data. If a set of modelled parameters were reached, it is believed to have great constraints for errors and could reasonably reflect the real properties of Se sorption processes (Bradbury and Baeyens, 1995, 1997, 2000).

Titration results can give information of site capacities and acid/base constants of the site protonation and deprotonation reactions, which are basic parameters for further sorption result simulations. Thus, the titration results were considered first.

The sorption results of Se can provide information about the constants of reactions between different Se species and sorption sites. Two types of sorption sites will be discussed here in a surface complexation model, the strong sorption sites ($\equiv S^SOH$) and weak sorption sites ($\equiv S^WOH$). This approach is supported by the existence of multiple sites on the surface of biotite (Bradbury and Baeyens, 1997; Dähn et al.,

2011; Zheng et al., 2003). The strong sorption sites ($\equiv S^SOH$) are considered having small capacities but strong complexes with sorbate. Strong sorption sites ($\equiv S^SOH$) will dominate the sorption when the sorbate is in a trace amount. The weak sorption sites ($\equiv S^WOH$), on the contrary, have much larger capacities, but much weaker complex abilities. The weak sorption sites ($\equiv S^WOH$) are believed to have dominant effects when the solution ions are in large concentrations.

Two types of weak sorption sites ($\equiv S^{W1}OH$ and $\equiv S^{W2}OH$) and one type of strong sorption sites ($\equiv S^SOH$) were assumed to exist on biotite surfaces based on molecular modelling results performed by quantum mechanics CASTEP (CAmbridge Serial Total Energy Package) code. The molecular modelling results were calculated by solving the total electronic energy and overall electronic density distribution in order to define the energetically stable structures (Clark et al., 2009; Leach, 2001; Puhakka et al., 2017; Puhakka and Olin, 2014). The modelling results show that two types of weak sorption sites exist on biotite surfaces (base (001) surface and edge (110) edge surface) with the site densities of 3.2 sites/nm^2 and 1.4 sites/nm^2, respectively.

For all the fitting and optimisation processes, a code that coupled PHREEQC with Python was developed (Charlton and Parkhurst, 2011; Liu et al., 2014; Wissmeier and Barry, 2011). PHREEQC is a computer program that is designed to perform a wide variety of aqueous geochemical calculations like speciation, sorption reactions, one-dimensional (1-D) transport and inverse geochemical calculations. Python is an open source and high-level programming language. It has an extensive ecosystem of scientific libraries and environments, and it has great performance due to close integration with time-tested and highly optimized codes written in C and Fortran. All these features make Python a suitable language for scientific computing. To facilitate interaction between PHREEQC and Python, a Microsoft COM (component object model) and COM version of PHREEQC called Iphreeqc were used. COM provides a server that allows PHREEQC to be used by any software that can interface with a COM server – for example, Excel, Visual Basic, Python and MATLAB. Iphreeqc is a version of PHREEQC that is specially designed for coupling to other programming codes and here it is coupled with Python for the fitting and optimization of the modelling results. While it retains all of PHREEQC reaction capabilities, Iphreeqc provides additional methods for data manipulation and communication to the host application (Charlton and Parkhurst, 2011; Wissmeier and Barry, 2011).

The modelling was performed by fitting titration, sorption edge and sorption isotherm data in an iterative procedure. Any parameter fitted in the present step will be fixed in all the subsequent steps. The iterative procedure breaks out if no satisfying fitting result can be reached. Then the modelling process returns to the first step with different parameters and begin the iteration again. The iteration ends when a group of parameters is found to be able to describe all the experimental results successfully (the squares of the difference between experimental data and simulated data $< 10^{-4}$).
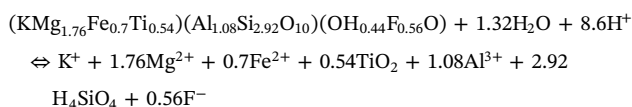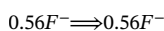
3. Results and modelling

3.1. Titration

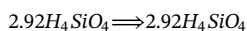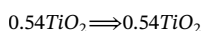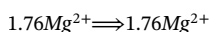In the studies of mineral surface site capacities and intrinsic surface protonation and deprotonation constants for amphoteric $\equiv SOH$ type surface sites, batch forward titration combined with the backtitration of the supernatants is more favored instead of continuous titration. The main problem of continuous titration is that it ignores the H$^+$/OH$^-$ consumption arising from the dissolution of minerals, which is quite significant at extreme pH values (pH $>$ 10 and pH $<$ 5). The ignorance of mineral dissolutions, together with other proton consuming or releasing mechanisms (such as proton and cation exchange reactions that we will show later) will cause two high H$^+$/OH$^-$ consumption in extreme pH areas.

To overcome the problem of mineral dissolution during titration,

researchers pointed out a batch backtitration method which could compensate the amount of mineral dissolved (Baeyens and Bradbury, 1995a, 1995b; Bradbury and Baeyens, 1995; Schulthess and Sparks, 1986). In this method, the supernatants from forward titration samples are back-titrated to a common end point. The quantities of acid or base consumed in the backtitration are subtracted from the quantities of the base or acid consumed in the forward titration. The theory can be explained by the following. In our case, biotite, in the minerals composition of $(KMg_{1.76}Fe_{0.7}Ti_{0.54})(Al_{1.08}Si_{2.92}O_{10})(OH_{0.44}F_{0.56}O)$, will dissolve in forward titration process and the dissolution reaction can be described by

$$(KMg_{1.76}Fe_{0.7}Ti_{0.54})(Al_{1.08}Si_{2.92}O_{10})(OH_{0.44}F_{0.56}O) + 1.32H_2O + 8.6H^+$$
$$\Leftrightarrow K^+ + 1.76Mg^{2+} + 0.7Fe^{2+} + 0.54TiO_2 + 1.08Al^{3+} + 2.92$$
$$H_4SiO_4 + 0.56F^-$$

8.6 mol H^+ are consumed by the dissolution of 1 mol biotite. In the backtitration, OH^- is consumed by the reaction products to reach a neutral pH and the following species are formed

$$K^+ \Longrightarrow K^+$$

$$1.76Mg^{2+} \Longrightarrow 1.76Mg^{2+}$$

$$0.7Fe^{2+} + 1.4OH^- \Longrightarrow 0.7Fe(OH)_2$$

$$0.54TiO_2 \Longrightarrow 0.54TiO_2$$

$$1.08Al^{3+} + 3.24OH^- \Longrightarrow 1.08Al(OH)_3$$

$$2.92H_4SiO_4 \Longrightarrow 2.92H_4SiO_4$$

$$0.56F^- \Longrightarrow 0.56F^-$$

4.64 mol OH^- are consumed by backtitration to neutral pH. This leaves 3.96 mol H^+ per mol of dissolved biotite not accounted for by backtitration. This part of H^+ should be added to the backtitration data.

Similarly, in the basic direction, 2.96 mol OH^- are consumed by the dissolution of 1 mol biotite while 6.92 mol H^+ are consumed by backtitration, indicating 3.96 mol H^+ more are consumed in the backtitration.

The chemical analysis results of Si and Al in the supernatants after titration show that the concentrations of Si and Al rise sharply at pH ≤ 5 and pH ≥ 10 (Fig. 1), indicating severe dissolution of biotite in the extreme pH conditions. The amounts of Si and Al remain constant at neutral pH (pH 6–8), which could be regarded as the background concentrations of these two elements. Thus, the difference between the concentrations of Si and Al at pH ≤ 5 and pH ≥ 10 and the background concentrations could be considered as the dissolved amounts of these
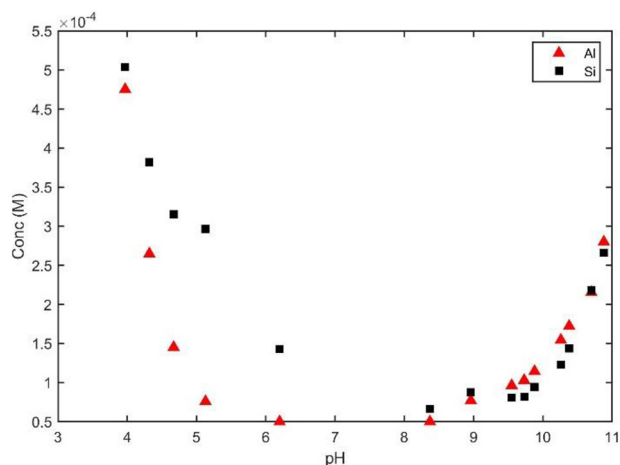

Fig. 1. Concentration of Al and Si elements in supernatants as a function of pH after forward titration of converted biotite in 0.01 M KClO₄.

two elements. Based on these assumptions together with the batch titration theory mentioned above, the correction of the H^+ and OH^- consumed in the backtitration can be calculated (Table 1).

However, the whole H^+/OH^- consumption in the batch forward titration cannot be compensated by just backtitration, especially in the extreme pH regions. Other factors, mainly proton exchange and cation exchange reactions between the dissolved cations and the biotite surface K^+, have effects on the titration process as well. If we simplify the biotite mineral as $M(OH)_3$, the process of cation exchange can be described by the following:

In the forward titration, $M(OH)_3$ dissolves and consumes H^+:

$$M(OH)_3 + 3H^+ \Longleftrightarrow M^{3+} + 3H_2O$$
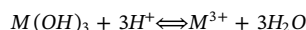
In the backtitration, dissolved M^{3+} ions are titrated to the neutral pH:

$$M^{3+} + 3OH^- \Longleftrightarrow M(OH)_3$$
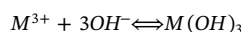
In the ideal situation, the amount of OH^- consumed could indicate all the amount of H^+ consumed by mineral dissolution. However, the fact is that, part of the M^{3+} will exchange with the surface K^+ and will be removed from the solution. The reaction can be written as:

$$3K\_biotite + M^{3+} \Longleftrightarrow M\_biotite + 3K^+$$
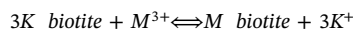
For example, Puhakka and Olin studied the cation exchange reactions of Ni^{2+} with the K^+ on the iron-rich biotite (annite) surfaces. The results show that K^+ will be replaced by Ni^{2+} on the basal surfaces of biotite (Puhakka and Olin, 2014).

The exchanged cations will not be accounted for by the backtitration. Following Gaines & Thomas convection (Gaines and Thomas, 1953), the ion exchange selectivity coefficient is defined by:

$$K_{N/M}^{G-T} = \frac{[M_{biotite}][K^+]^3}{[K_{biotite}]^3[M^{3+}]}$$

where $[M_{biotite}]$ and $[K_{biotite}]$ represent the equivalent fraction of the corresponding sites. $[K^+]$ and $[M^{3+}]$ are the concentrations of different cations.

Similarly, the proton exchange reaction can be described by:

$$K\_biotite + H^+ = H\_biotite + K^+$$
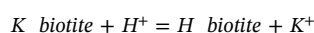
and the selectivity coefficient can be defined by Gaines & Thomas convection as shown above.

By recording the cation exchange abilities of different cations with K^+ on biotite surface, the corresponding selectivity coefficients of the cation exchange reactions could be measured (Table 2). The selectivity coefficient of the proton exchange reaction is assumed to be one, since the study of the exchange reactions of hydrogen ions is greatly complicated because of the instability of the mineral. This assumption was also adopted by other researches (Bradbury and Baeyens, 2009a, 2009b; Gilbert and Laudelout, 1965).

The CEC of converted biotite was determined by checking the end point of the cation exchange curve of Al^{3+} which has the largest cation exchange ability. There is a clear trend that the quantity of cation exchange ions is going to be saturated at the end point region (Fig. 2). A CEC value of 19.5 meq/kg was estimated and used in the selectivity coefficients calculations. The CEC value measured by ammonium acetate for non-converted biotite in our previous work with the same particle size from 0.075 mm to 0.3 mm was 12.64 meq/kg (Li et al., 2018).

Thus, the amount of sorption sites occupied by cations on the biotite surface at each pH could be calculated according to the measured equilibrium concentration of different cations in the supernatant and the CEC value (Table 3). The results show that Al^{3+} is the most abundant cation that is sorbed on the biotite surface. The quantities of other sorbed cations could be omitted in comparison with that of Al^{3+}. The quantities of proton exchange are also in a small amount. Based on the results in Table 3, Al^{3+} and H^+ occupancies are going to be used for

Table 1

Summary of the titration, backtitration and dissolution correction data according to dissolved concentration of Si in extreme pH regions. The background concentration of Si is 6.6×10^{-5} mol/L. The dissolution corrected consumption is calculated by the subtraction of forward titration with backtitration and mineral dissolution (the column of H^+/OH^- correction for backtitration).

pH	Forward titration (mol)	Backtitration (mol)	Dissolved Si (mol)	Dissolved biotite (mol)	H^+/OH^- correction for backtitration (mol)	Dissolution corrected consumption (mol)
Acid titration						
5.13	3.2E-05	7.7E-06	5.8E-06	2.0E-06	7.8E-06	1.7E-05
4.67	4.3E-05	1.4E-05	6.2E-06	2.1E-06	8.4E-06	2.1E-05
4.32	6.0E-05	2.7E-05	7.9E-06	2.7E-06	1.1E-05	2.2E-05
3.97	8.5E-05	4.4E-05	1.1E-05	3.7E-06	1.5E-05	2.6E-05
Base titration						
10.26	1.5E-05	9.7E-06	1.4E-06	4.9E-07	1.9E-06	7.3E-06
10.38	2.0E-05	1.3E-05	1.9E-06	6.6E-07	2.6E-06	9.3E-06
10.70	3.0E-05	2.3E-05	3.8E-06	1.3E-06	5.1E-06	1.3E-05
10.88	4.0E-05	3.3E-05	5.0E-06	1.7E-06	6.8E-06	1.4E-05

Table 2

Cation exchange reactions of the dissolved cations with biotite surface K^+ and the calculated selectivity coefficients according to the Gaines and Thomas convection.

Cation exchange reaction	Selectivity coefficients (K)
K-biotite + H^+ = H-biotite + K^+	1 (logK = 0)
K-biotite + Na^+ = Na-biotite + K^+	3.4
2 K-biotite + Mg^{2+} = Mg-biotite + 2 K^+	0.16
2 K-biotite + Ca^{2+} = Ca-biotite + 2 K^+	0.17
3 K-biotite + Al^{3+} = Al-biotite + 3 K^+	0.59

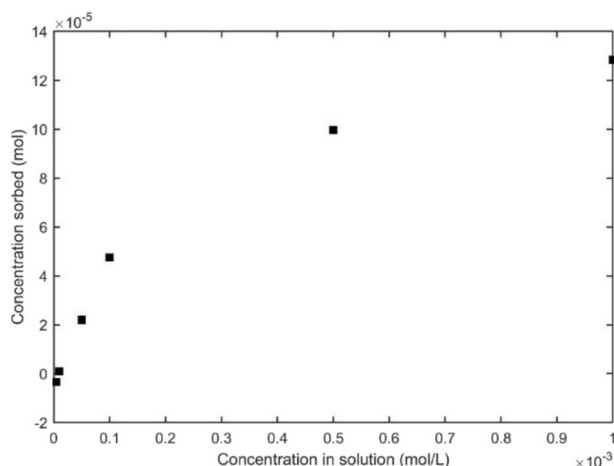**Fig. 2.** The amount of Al^{3+} sorbed on the surface of concerted biotite as a function of aqueous Al^{3+} concentration from 5×10^{-6} M to 1×10^{-3} M.

Table 3

The amount of sorption sites occupied by cations on converted biotite calculated using the selectivity coefficients listed in Table 2 with CEC value of 19.5 meq/Kg.

pH	Cation occupancies (meq/Kg)					
	H	K	Ca	Mg	Na	Al
5.13	0.0037	4.9	0.029	0.120	0.028	14.4
4.67	0.0087	4.1	0.020	0.096	0.190	15.1
4.32	0.016	3.4	0.012	0.076	0.013	16.0
3.97	0.030	2.8	0.009	0.060	0.075	16.5

corrections of cation exchange and proton exchange effects.

A summary of the forward titration, backtitration, cation exchange, proton exchange and net consumed H^+/OH^- data are shown in Table 4. The quantities of the net consumed H^+ or OH^- are calibrated by all the

factors mentioned above: backtitration, mineral dissolution, cation exchange and proton exchange. The results show that backtitration is the main calibration for the forward titration data. This proves that mineral dissolution occurred during the titration processes and introduced errors into the titration data and continuous titration is not suitable for titrating minerals like biotite. Comparing with backtitration, the contributions of the calibrations of cation exchange and proton exchange to the titration curve are insignificant. However, Bradbury and Baeyens pointed out in their earlier work that the relative importance of H^+ and Al^{3+} depends sensitively on the background electrolyte concentration and type, and increases in importance as the ionic strength decreases (Bradbury and Baeyens, 2009a, 2009b, 2005a, 2005b). In this work, the background electrolyte is 0.01 M $KClO_4$, which can be regarded as a low concentration. The biggest contribution of cation exchange and proton exchange is ~7% at pH 5.13.

The titration results were modelled in terms of protonation reactions. The sorption of Se on biotite happens through surface complexation mechanism, i.e. on the hydroxyl surface functional groups ($\equiv SOH$) which are amphoteric and exist at broken bonds and edge sites on mineral surfaces (Li et al., 2018; Rovira et al., 2008; Söderlund et al., 2016b). In essence, a titration plot is a proton adsorption and desorption isotherm for the $\equiv SOH$ sites. A quantitative understanding about the acid/base behaviour of surface binding sites is critical for any model description. The proton sorption and desorption behaviours of the sorption sites ($\equiv SOH$) could be modelled in terms of protonation reactions:
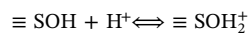
$$\equiv SOH + H^+ \Longleftrightarrow \equiv SOH_2^+$$

and deprotonation reactions:
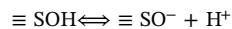
$$\equiv SOH \Longleftrightarrow \equiv SO^- + H^+$$

The reaction constants can be described without an electrostatic term like,

$$K_{protonation} = \frac{[\equiv SOH_2^+]}{[\equiv SOH] \cdot \{H^+\}}$$

and

$$K_{deprotonation} = \frac{[\equiv SO^-] \cdot \{H^+\}}{[\equiv SOH]}$$

respectively, where [] represents concentrations in M and {} represents activities.

As described earlier, the sorption site densities of two types of weak sorption sites were calculated by molecular modelling, while the sorption site density of the strong sorption sites was estimated by the fitting of sorption isotherm data, which will be discussed later. The general parameters that were used for the titration modelling as well as the sorption edge and sorption isotherm modelling later are shown in Table 5. These basic parameters were fixed for the whole modelling

Table 4
Summary of the forward titration, backtitration, minerals dissolution calibration, cation exchange, proton exchange data for plotting the titration curve. The experiments were carried out with 0.5 g converted biotite and 25 mL 0.01 M KClO$_4$ (solid to liquid ratio: 20 g/L). The quantities of the net consumed H$^+$ or OH$^-$ are calibrated by backtitration, mineral dissolution, cation exchange and proton exchange.

pH	Acid/Base added (mol)	Backtitration added (mol)	Mineral dissolution (mol)	Cation exchange (mol)	Proton exchange (mol)	Net consumed (mol)
Acid						
6.41	7.0E-06	3.3E-07	–	–	–	6.7E-06
6.05	1.1E-05	1.3E-06	–	–	–	9.7E-06
5.72	1.3E-05	2.0E-06	–	–	–	1.1E-05
5.38	1.7E-05	4.0E-06	1.7E-06	–	–	1.1E-05
5.35	1.6E-05	3.8E-06	1.9E-06	–	–	1.1E-05
5.13	3.2E-05	7.7E-06	7.8E-06	2.4E-06	1.8E-09	1.4E-05
4.67	4.3E-05	1.4E-05	8.4E-06	2.5E-06	4.3E-09	1.8E-05
4.32	6.0E-05	2.7E-05	1.1E-05	2.7E-06	8.1E-09	2.0E-05
3.97	8.5E-05	4.4E-05	1.5E-05	2.8E-06	1.5E-08	2.3E-05
3.50	9.3E-05	4.6E-05	1.9E-05	2.9E-06	1.9E-08	2.5E-05
Base						
8.37	2.2E-06	1.7E-06	–	–	–	4.8E-07
8.96	4.0E-06	1.7E-06	7.3E-07	–	–	3.1E-06
9.55	7.0E-06	2.8E-06	4.8E-07	–	–	4.7E-06
9.73	8.0E-06	3.8E-06	5.2E-07	–	–	4.8E-06
9.88	1.0E-05	5.0E-06	9.6E-07	–	–	6.0E-06
10.26	1.5E-05	9.7E-06	1.9E-06	–	–	7.3E-06
10.38	2.0E-05	1.3E-05	2.6E-06	–	–	9.3E-06
10.70	3.0E-05	2.3E-05	5.1E-06	–	–	1.3E-05
10.88	4.0E-05	3.3E-05	6.8E-06	–	–	1.4E-05

Table 5
General parameters used in titration and sorption data modelling. SSA, Mass and CEC data are measured from experiments. The sorption site densities of two weak sorption sites ($\equiv$S^{W1}OH and $\equiv$S^{W2}OH) are from molecular modelling results while the sorption site density of the strong sorption site ($\equiv$S^{S}OH) is the optimized modelling parameter.

Parameter	Biotite
SSA(m^2/g)	1.0323
Mass (g)	0.5
Sorption site densities (sites/nm^2)	0.00068 ($\equiv$S^{S}OH)
	3.2 ($\equiv$S^{W1}OH)
	1.4 ($\equiv$S^{W2}OH)
CEC (meq/Kg)	12.64

procedures.

The modelled protonation and deprotonation reaction constants for the strong sorption sites and two types of weak sorption sites are shown in Table 6 and the results are shown in Fig. 3 with experimental data for comparison. One thing should be mentioned for the calculated results is that it is assumed that the protonation/deprotonation reaction constants for strong sorption sites ($\equiv$S^{S}OH) is the same as those for the first type of weak sorption sites ($\equiv$S^{W1}OH) (Ervanne et al., 2013; Missana et al., 2009; Wang et al., 2001). The reason for assuming this is that the unknown parameters are too many without this assumption, which creates too much uncertainty and unpredictability to the modelling results.

The site types and site densities as well as the corresponding

Table 6
Protonation and deprotonation reaction of hydroxyl surface functional groups ($\equiv$SOH) and the corresponding reaction constants of biotite in 0.01 M KClO$_4$.

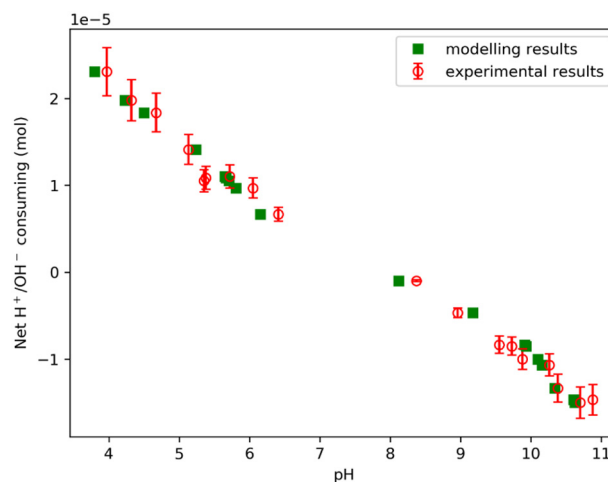| Reactions	logK
$\equiv$S^{S}OH + H$^+$ $\Longleftrightarrow$ $\equiv$ S^{S}OH$_2{}^+$	5.05
$\equiv$S^{S}OH $\Longleftrightarrow$ $\equiv$ S^{S}O$^-$ + H$^+$	−8.78
$\equiv$S^{W1}OH + H$^+$ $\Longleftrightarrow$ $\equiv$ S^{W1}OH$_2{}^+$	5.05
$\equiv$S^{W1}OH $\Longleftrightarrow$ $\equiv$ S^{W1}O$^-$ + H$^+$	−8.78
$\equiv$S^{W2}OH + H$^+$ $\Longleftrightarrow$ $\equiv$ S^{W2}OH$_2{}^+$	6.10
$\equiv$S^{W2}OH $\Longleftrightarrow$ $\equiv$ S^{W2}O$^-$ + H$^+$	−11.22

Fig. 3. Titration experimental data for Se(IV) sorption on converted biotite in 0.01 M KClO$_4$ solution from pH 3 to pH 11 (●) and the modelling results (■).

protonation and deprotonation constants play a central role in the sorption data modelling. The set of parameters describing the amphoteric behaviours of $\equiv$SOH type sites will become non-adjustable parameters in all the following modelling approaches.

3.2. Sorption edge

The sorption edge measurements were carried out by measuring the sorption of 10^{-9} M total Se with a radioactive Se-75 tracer on converted biotite in 0.01 M KClO$_4$ solution. The tested Se is in +IV oxidation state (Se(IV)). According to the previous work (Li et al., 2018), Se(IV) will not be oxidized to +VI state or reduced to elementary selenium during the experiments. The sorption edge experimental results (Fig. 4) show that the sorption of Se on biotite surfaces decreases as pH increases from 3 to 8, while in the basic region, the K_d values decrease to near 0 and the sorption was considered negligible in comparison with the sorption in the acidic region. In the deep groundwater conditions of granitic rock, the water is usually in a slightly basic state (7–10), which makes Se a highly mobile element.
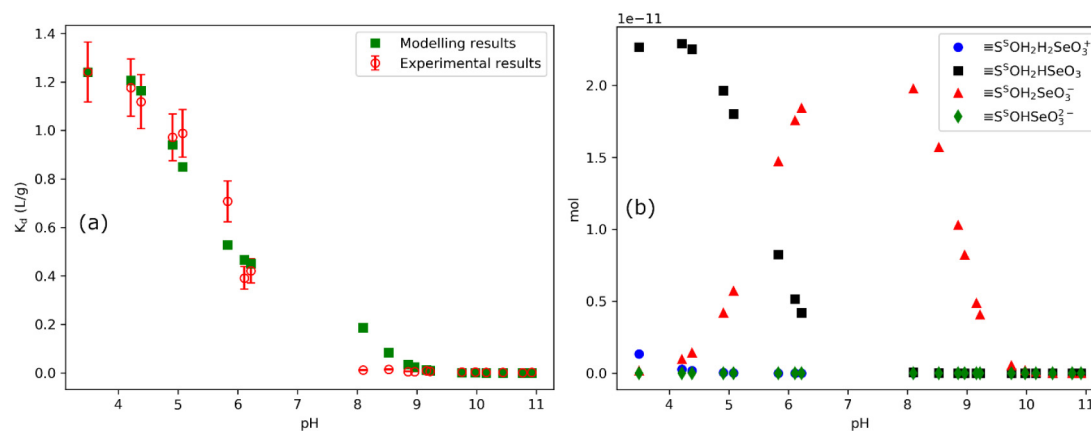
Fig. 4. a) Sorption edge data (●) of 10^{-9} M Se(IV) on 0.5 g converted biotite in 25 mL 0.01 M KClO$_4$ solution from pH 3 to 11 and the modelling results (■) with strong sorption sites. b) The modelled moles of different sorption species on the surface of biotite as a function of pH from 3 to 11.

Two main sorption mechanisms, ion exchange and surface complexation, are considered influencing the sorption of radioelements on mineral surfaces. Ion exchange sites originate from the isomorphous substitution of lattice elements, causing permanent negative or positive charge regions on the surface of mineral platelets. Charge neutrality is maintained by the presence of an excess of counter-charge ions in solution held electrostatically in close proximity. The electrostatically bound ions can undergo exchange with the ions in solution. This kind of sorption mechanism has a weak dependency on pH except at low pH (Bradbury and Baeyens, 2002, 2009a). However, Fig. 4 shows a strong pH dependency of Se sorption, which indicates the fitting of the second sorption mechanism, i.e. surface complexation. Surface complexation happens to nuclide bounding on sorption sites which are perceived as being surface hydroxyl groups ($\equiv$SOH). The $\equiv$SOH groups can undergo protonation ($\equiv SOH_2^+$) and deprotonation ($\equiv SO^-$) reactions, depending on the pH conditions of background solutions. The protonation and deprotonation properties of the sorption sites have been analyzed by titration experiments in the above section.

In the modelling of Se sorption edge process, only the uptake on strong sorption sites was considered because of the very low concentration of tracer ions used in the experiments (10^{-9} M). The two model parameters required to calculate sorption edge are the $\equiv$S^{S}OH site density and the surface complexation reaction constant K. The aqueous speciation of Se will play an import role in the sorption edge modelling because different Se species with three different valences (SeO_3^{2-}, $HSeO_3^-$, H_2SeO_3) exist in the experimental pH range from 3 to 11, as shown in Fig. 5a. The figure was calculated based on the speciation data from Ervanne et al. (2016) and shown in Table 7.
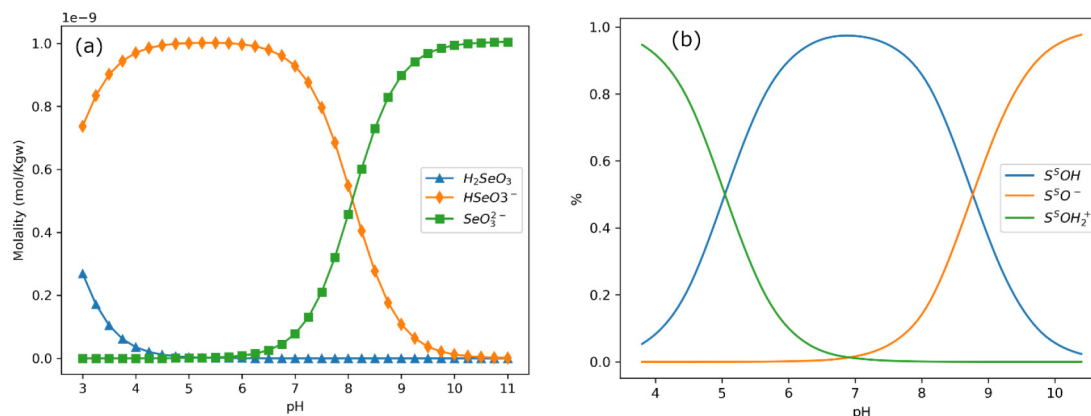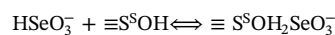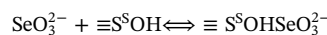
Table 7
Se species and speciation reactions expected in 0.01 M KClO$_4$ solution. The thermodynamic equilibrium constants were cited from Ervanne et al. (2016).

Speciation reaction	Log K
$H^+ + HSe^- = H_2Se$	3.8
$HSe^- = Se^{2-} + H^+$	-14
$H^+ + SeO_3^{2-} = HSeO_3^-$	8.54
$2H^+ + SeO_3^{2-} = H_2SeO_3$	11.24
$H^+ + SeO_4^{2-} = HSeO_4^-$	1.8
$2H^+ + SeO_4^{2-} = H_2SeO_4$	-0.21

Fig. 5b shows the distribution of strong sorption sites under different pH conditions calculated based on the data in Table 7. The aqueous speciation and sites distribution provides a guide for choosing reasonable surface complexation reactions. For most of the pH range, $HSeO_3^-$ and SeO_3^{2-} are the two dominant species in the background solution. The surface complexation reactions representing the sorption of the two species on $\equiv$S^{S}OH will be identified first:

$$SeO_3^{2-} + \equiv S^SOH \Longleftrightarrow \equiv S^SOHSeO_3^{2-}$$

$$HSeO_3^- + \equiv S^SOH \Longleftrightarrow \equiv S^SOH_2SeO_3^-$$

In the acidic area, the protonated sorption hydroxyl groups $\equiv SOH_2^+$ will become popular and the complexation reaction with $HSeO_3^-$ happens (The amount of SeO_3^{2-} is insignificant in the acid environments and the complexation of SeO_3^{2-} with $\equiv SOH_2^+$ will be omitted). The complexation will be expressed as:

Fig. 5. a) Se speciation calculated as a function of pH. The whole concentration of Se is set to be 1×10^{-9} M. Redox processes were not taken into account in the calculations. b) The strong sorption sites distribution as a function of pH.

Table 8

Surface complexation reactions of different Se species on strong sorption sites and the related reaction selectivity coefficients used in the modelling of sorption edge results.

Reactions	log K
$SeO_3^{2-} + \equiv S^SOH \Longleftrightarrow \equiv S^SOHSeO_3^{2-}$	−2.23
$HSeO_3^- + \equiv S^SOH \Longleftrightarrow \equiv S^SOH_2SeO_3^-$	7.89
$H^+ + HSeO_3^- + \equiv S^SOH \Longleftrightarrow \equiv S^SOH_2HSeO_3$	13.46
$H^+ + H_2SeO_3 + \equiv S^SOH \Longleftrightarrow \equiv S^SOH_2H_2SeO_3^+$	13.02

$$H^+ + HSeO_3^- + \equiv SOH \Longleftrightarrow \equiv S^SOH_2HSeO_3$$
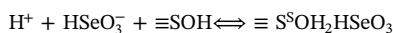
Also, in strong pH region (pH < 4), the amount of H_2SeO_3 species could not be neglected. The complexation between $\equiv S^SOH_2^+$ and H_2SeO_3 should also be considered:

$$H^+ + H_2SeO_3 + \equiv S^SOH \Longleftrightarrow \equiv S^SOH_2H_2SeO_3^+$$

The selectivity coefficients of the strong sorption sites, K^S, for the surface complexation reactions could be expressed like:

$$K^S_{SeO_3^{2-}} = \frac{[\equiv S^SOHSeO_3^{2-}]}{\{SeO_3^{2-}\} \cdot [\equiv S^SOH]}$$

where $K_{SeO_3^{2-}}{}^S$ is the complexation selectivity coefficient, and [] the concentration of sorption sites and {} the activity of aqueous species. The selectivity coefficients $K_{HSeO_3^-}{}^S$, $K_{H_2SeO_3}{}^S$ and $K_{H_3SeO_3^+}{}^S$ have similar expressions.

The modelled sorption edge data shown in Fig. 4a are based on the selectivity coefficients listed in Table 8 which have been optimized by the least squares method (best fit). Comparing the selectivity coefficients calculated, which indicate the abilities/possibilities of surface reactions, the reaction between SeO_3^{2-} and $\equiv S^SOH$ is the most difficult to happen (logK = −2.23), while the reaction between $HSeO_3^-$ and $\equiv S^SOH$ happens more easily (logK = 7.89). The calculated moles of different sorption species on the surface of converted biotite are illustrated in Fig. 4b. It shows that the production of $\equiv S^SOHSeO_3^{2-}$ which results from the reaction between $\equiv S^SOH$ and SeO_3^{2-} is quite low and it will not cause obvious influence for K_d values if pH is below 10. At pH conditions between 6 and 10, the main sorption species on biotite surface is $\equiv S^SOH_2SeO_3^-$ which results from the reaction between $\equiv S^SOH$ and $HSeO_3^-$. This is the most important reaction that occurs under the conditions of deep geological repository. If pH is below 5, the main sorption species on biotite surface becomes $\equiv S^SOH_2HSeO_3$ which is the production of H^+, $HSeO_3^-$ and $\equiv S^SOH$. This might be important process in surface water conditions. The $\equiv S^SOH_2H_2SeO_3^+$ species will appear only under pH 5 and may become important under acidic conditions. The inconsistence between the modelled and experimental results was found between pH 8 and 9 due to reactions between $\equiv S^SOH$ and $HSeO_3^-$. However, the modelled and calculated results are in good agreement under other pH conditions.

The order of the selectivity coefficients corresponds to the determined sorption energies of different Se species calculated by molecular modelling (Puhakka et al., 2017). The modelling is based on solving the total electronic energy and overall electronic density distribution in order to define the energetically stable structures of minerals and sorption species. Exothermic sorption energies indicate that surface complexation reactions are presumable. Based on molecular modelling results, $HSeO_3^{2-}$ and H_2SeO_3 could form the very stable complexes on the edge surfaces of biotite (Table 9). However, it has to be stated that the neutral Se species do not occur in the natural groundwater conditions in the bedrock or our batch sorption experiments (pH 8). Therefore, the most probable Se species in the sorption reaction is $HSeO_3^-$.

Fig. 6 shows the sorption geometries for the investigated Se species. Sorption of SeO_3^{2-} happens onto the surface via its oxygen atoms to the hydrogen atoms of the surface hydroxyl groups (Fig. 6a). Further,

Table 9

Sorption energies (eV) of the Se species onto the biotite (phlogopite) surfaces.

Se species	Phlogopite			
	$S^S(110)$	$S^W(110)$	$S^W(110)$	$S^W(001)$
	–O–Se	–O–Se	–Se–O	–O–Se
$Se(IV)O_3^{2-}$	1.3	4.6	6.4	5.7
$HSe(IV)O_3^-$	−2.7	−1.8	4.5	3.4
$H_2Se(IV)O_3$	−4.6	−5.2	0.7	−2.3

SeO_3^{2-} reacts with the surface hydroxyl groups taking on a proton to itself and forming the $HSeO_3^-$ species. On the weak sorption site, SeO_3^{2-} remains unchangeable (Fig. 6b). During the sorption of $HSeO_3^-$, Se species gives up its oxygen atom to the surface. After the replacement of the surface hydroxyl groups, reaction releases water like the S_N2-I reaction mechanism predicts, and $HSeO_3^-$ transfers to the cationic $HSeO_2^+$ species. The reaction is similar on both sorption sites (Fig. 6c and Fig. 6d). When neutral H_2SeO_3 species adsorbs onto the surface, cationic $HSeO_2^+$ species forms and water is released (Fig. 6e and Fig. 6f). The results reveal that electron transfer reactions happen between the biotite surface and Se species, and all these sorption reactions happen spontaneously.

3.3. Sorption isotherm

The sorption isotherm experimental results (Fig. 7) show that a clear increasing trend exists for K_d values with the decrease of Se concentration; however, a drastic increase happens when the Se concentration decreases from 10^{-7} M to 10^{-8} M. Two platforms could be observed in the low concentration area (10^{-10} M to 10^{-8} M) and high concentration area (10^{-7} M to 10^{-3} M). This may indicate different sorption mechanisms when the concentration changed. The K_d values stabilized at 0.01–0.02 m^3/kg in the high concentration area and at 0.06–0.07 m^3/kg in the low concentration area.

Sorption isotherms for Se on biotite were measured at slightly basic environments (pH ~ 7.7) over concentration ranges from 10^{-10} M to 10^{-3} M. All the strong sorption site parameters, including surface site density and surface reactions derived from the sorption edge modelling were fixed. The surface reactions of Se species between the two types of weak sorption sites are the remaining unknown parameters at this stage.

According to the Se speciation distribution calculations (Fig. 5), $HSeO_3^-$ is the dominant Se species at the experimental conditions. Furthermore, as shown by the sorption edge modelling results (Fig. 4), the reactions between $\equiv S^SOH$ and $HSeO_3^-$ and the reaction between $\equiv S^SOH$, H^+ and $HSeO3^-$ are the main reactions from pH 7 to 10. Thus, $HSeO_3^-$ will be considered as the main reactant with the two weak sorption sites which determines the main shape of the isotherm curve in high concentration area. Table 10 shows the surface complexation reactions between $HSeO_3^-$ and $\equiv S^{W1}OH/ \equiv S^{W2}OH$ together with the optimized logK values.

The modelling results of site occupations indicate that the strong sorption sites with a low site density of 0.00068 sites/nm^2, dominate the Se(IV) sorption in the low concentration area ($< 10^{-8}$ M). However, with the increase of Se(IV) concentration, the contribution of the weak sorption sites becomes more important due to the low site density of the strong sorption sites. The mechanisms of the strong sorption sites are still under discussion. Dähn et al. (2011) illustrates that strong sorption happens onto the mineral surface as a mixture of surface complexes bound to the edge sites of the *cis*-vacant (cv) and *trans*-vacant (tv) of Al octahedrons. However, more evidence is needed to understand the true nature of the so-called "strong" sorption site in the case of Se(IV) sorption on biotite.
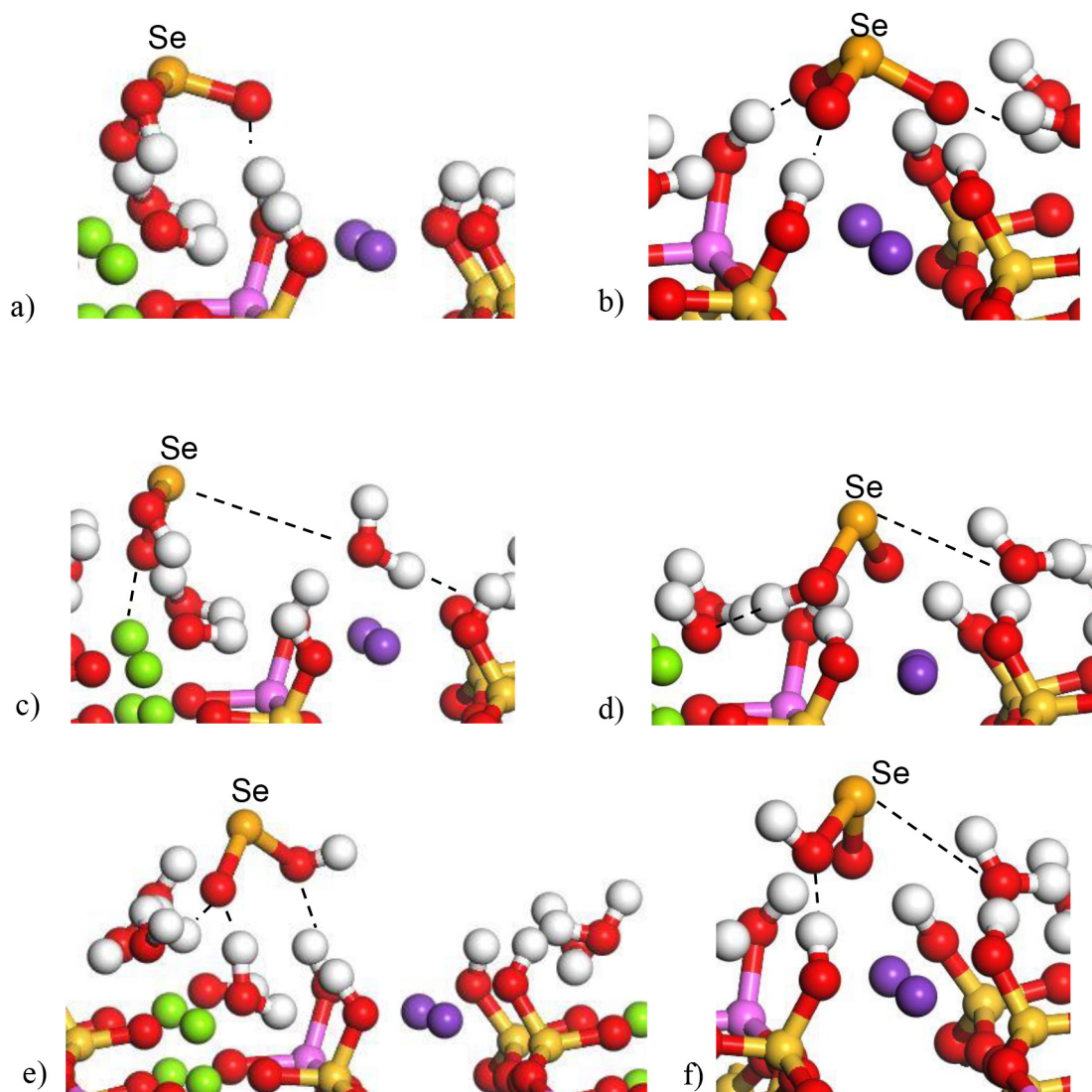
Fig. 6. Sorption of SeO_3^{2-} (a and b), $HSeO3^-$ (c and d) and H_2SeO_3 (e and f) onto the phlogopite (110) surface.
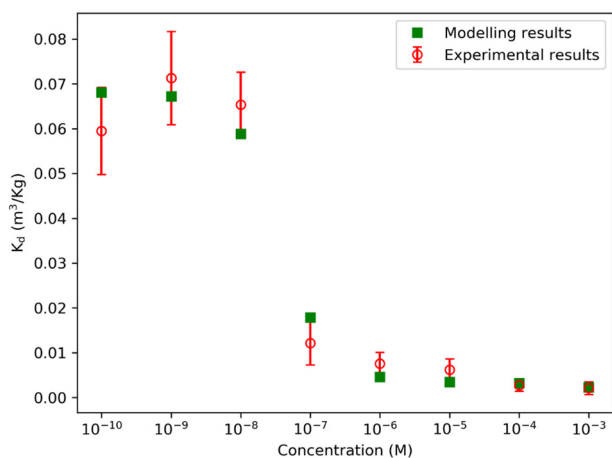

Fig. 7. Se(IV) sorption isotherm data (●) on converted biotite in 0.01 M $KClO_4$ solution covering Se(IV) concentration from 10^{-10} M to 10^{-3} M. The modelling results (■) were based on the sorption of Se(IV) species on the strong sorption sites ($\equiv S^SOH$) and two types of weak sorption sites ($\equiv S^{W1}OH$ and $\equiv S^{W2}OH$).

Table 10

Expected surface complexation reactions between Se(IV) species and weak sorption sites on converted biotite surface at pH around 7.7. The selectivity coefficients were optimized from the modelling of sorption isotherms.

Surface complexation reaction	log K
$HSeO_3^- + \equiv S^{w1}OH \Longleftrightarrow \equiv S^{w1}OH_2SeO_3^-$	2.78
$H^+ + HSeO_3^- + \equiv S^{w1}OH \Longleftrightarrow \equiv S^{w1}OH_2HSeO_3$	3.78
$HSeO_3^- + \equiv S^{w2}OH \Longleftrightarrow \equiv S^{w2}OH_2SeO_3^-$	2.48
$H^+ + HSeO_3^- + \equiv S^{w2}OH \Longleftrightarrow \equiv S^{w2}OH_2HSeO_3$	2.62

3.4. Model validations

To validate the surface complexation model, especially to test the feasibility of the model at pH 9.5 which is the pH of the Grimsel groundwater (Hoehn et al., 1998; Muuri et al., 2018; Tachi et al., 2015), another batch sorption experiment was done with the same experimental conditions except for pH. In the validation experiments, the pH was adjusted to 9.5 by adding NaOH standard solution into the sample vials. The pH was checked and adjusted during the whole experimental period.

The modelling of the experimental results was done by optimizing the pH parameter while keeping the other parameters the same as the sorption isotherm modelling we presented in the last parts. The best fit
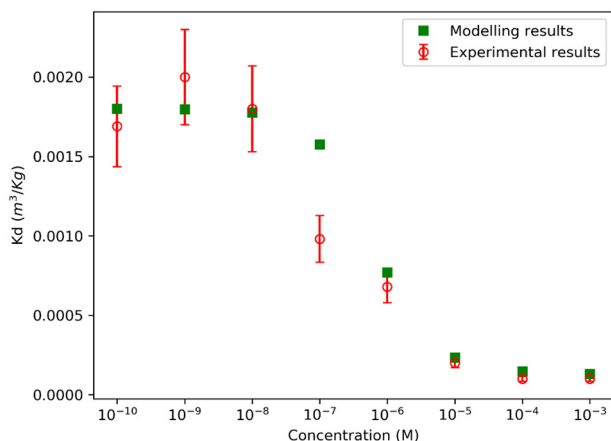
Fig. 8. Se(IV) sorption isotherm data (●) on converted biotite in 0.01 M KClO4 solution covering Se(IV) concentration from 10^{-10} M to 10^{-3} M at pH ~9.5. The modelling results (■) were based on the sorption of Se(IV) species on the strong sorption sites ($\equiv S^SOH$) and two types of weak sorption sites ($\equiv S^{W1}OH$ and $\equiv S^{W2}OH$) at pH 9.34.

was achieved at pH 9.34 which is in fare agreement with the experimental conditions. The experimental and modelling results are shown in Fig. 8.

The model predicted the K_d values well at both high and low concentration regions. At the concentration of 10^{-7} M, the sorption of Se (IV) on biotite is believed to be dominated by both strong and weak sorption sites. Our model showed a higher K_d value than the real experimental result. Except for the point at 10^{-7} M, the modelled results are all within the experimental errors. This means that the multi-site surface complexation model we developed here could be used to describe the Se(IV) sorption on biotite over a large pH ranges at least from pH 7.5 to 9.5 which covers most of the pHs of groundwaters in the bedrocks of a nuclear waste repository.

A sorption model developed with biotite is of significant importance because biotite can be representative of the whole Se(IV) sorption in complex mineral assemblages such as granite which is considered as the bedrocks of nuclear waste repositories (Li et al., 2018; Muuri et al., 2017; Yang et al., 2018). Such sorption model which provides quantitative predictions are necessary for developing thermodynamic sorption databases which is a major long-term goal in improving the scientific basis for nuclear water disposal. Furthermore, the model can be ported into reactive transport codes and the sorption on minerals like biotite can be calculated simultaneously with the transport, taking into account the effects of spatial and temporal changes in geochemical conditions along the migration path. Thus, the transport calculations are truer to nature and the performance assessment of the nuclear waste repository can give more convincing results to estimate the release of radionuclides towards aquifers and biosphere.

4. Conclusions

A batch forward titration method combined with backtitration was used to measure the mineral surface site capacities and intrinsic surface protonation and deprotonation constants for the amphoteric $\equiv SOH$ surface sites of converted biotite in 0.01 M $KClO_4$ solution and pH range from 3 to 11. In order to minimize the effect of impurities on the surface sites, the biotite was purified with ion exchange methods until the concentrations of Mg^{2+}, Ca^{2+} and Al^{3+} ions in the rinsing solutions were under the detection limit and the concentration of Na^+ was 0.06 ppm. By doing this, the biotite sample was converted into a mono-potassium form that contains only K on the exchange sites. During the backtitration, the supernatants from forward titration samples were back titrated to a common end point. By applying

backtitration, the effect of the mineral dissolution was taken into account, especially in extreme pH areas where the mineral dissolution is very obvious. The effects of proton exchange and cation exchange on the titration results were also taken into account. The calculations of the amount of sorption sites occupied by cations on the biotite surface show that dissolved Al^{3+} is the most abundant cation that is sorbed on the biotite surfaces. As a result, Al^{3+} and H^+ occupancies were used as further corrections of the titration curve.

Sorption edge measurements were carried out by measuring the sorption of 10^{-9} M total Se with a radioactive Se-75 tracer on converted biotite in 0.01 M $KClO_4$ solution from pH 3 to 11. Se(IV) sorption showed a strong dependency of pH conditions of background solutions. The K_d values of Se sorption on biotite were found to decrease when pH increases from 3 to 11.

Sorption isotherm measurements were carried out at around pH 7.7 from Se(IV) concentrations from 10^{-10} M to 10^{-3} M. Two platforms were observed in the low and high concentration regions. A clear change of K_d happened at concentration around 10^{-7} M.

A multi-site surface complexation model was derived by fitting a set of modelling parameters for all the experimental data (titration, sorption edge and sorption isotherm). It is believed that this set of modelled parameters can reasonably reflect the real properties of the sorption processes. A type of strong sorption site and two types of weak sorption sites were assumed. A CASTEP code implemented into Materials Studio Software was used to calculate the site densities and site types on the biotite surfaces. The results showed two types of weak sorption sites on the biotite surfaces with the site densities of 3.2 sites/nm^2 and 1.4 sites/nm^2. A computer code PHREEQC coupled with Python was used for all of the fitting and optimization processes. The fitting procedure was performed in an iterative way until a group of parameters that is able to describe all the experimental results satisfyingly was found.

The model was validated by the Se(IV) sorption data at pH ~9.5 and it describes well the K_d values at both high and low concentration regions. This proves that the modelling methods shown in this paper can be used to successfully derive a surface complexation model for sorption of the radionuclides on crystalline rock in deep geological repositories. In the future, the model could be used to validate the Se(IV) sorption in wide range of groundwater conditions.

Declaration of competing interest

The authors declare that they have no known competing financial interests or personal relationships that could have appeared to influence the work reported in this paper.

References

Altmann, S., 2008. Geochemical research: a key building block for nuclear waste disposal safety cases. J. Contam. Hydrol. 102, 174–179. https://doi.org/10.1016/j.jconhyd.2008.09.012.

Armarego, W.L.F., Chai, C.L.L., 2013. Purification of Laboratory Chemicals, 7th edition. .

Atwood, D.A., 2010. Radionuclides in the Environment. WILEY.

Baeyens, B., Bradbury, M.H., 1995a. A Quantitative Mechanic Description of Ni, Zn and Ca Sorption on Na-Montmorillonite Part I: Physico-Chemical Characterisation and Titration Measurements. Technical Report NTB 95–04 Nagra, Wettingen, Switzerland.

Baeyens, B., Bradbury, M.H., 1995b. A quantitative mechanistic description of Ni, Zn and Ca Sorption on Na-montmorillonite part II: sorption measurements. In: Technical Report NTB 95–05. Nagra, Wettingen, Switzerland.

Bradbury, M.H., Baeyens, B., 1995. A quantitative mechanistic description of Ni, Zn and

Ca sorption on Na-montmorillonite part III: modelling. In: Technical Report NTB 95–06. Nagra, Wettingen, Switzerland.

Bradbury, M.H., Baeyens, B., 1997. A mechanistic description of Ni and Zn sorption on Na-montmorillonite part II: modelling. J. Contam. Hydrol. 27, 223–248. https://doi.org/10.1016/S0169-7722(97)00007-7.

Bradbury, M.H., Baeyens, B., 2000. A generalised sorption model for the concentration dependent uptake of caesium by argillaceous rocks. J. Contam. Hydrol. 42, 141–163.

Bradbury, M.H., Baeyens, B., 2002. Sorption of Eu on Na- and Ca-montmorillonites: experimental investigations and modelling with cation exchange and surface complexation. Geochim. Cosmochim. Acta 66, 2325–2334. https://doi.org/10.1016/S0016-7037(02)00841-4.

Bradbury, M.H., Baeyens, B., 2005a. Experimental and Modelling Investigations on Na-Illite: Acid-Base Behaviour and the Sorption of Strontium, Nickel, Europium and Urany. Paul Scherrer Institut, Villigen PSI.

Bradbury, M.H., Baeyens, B., 2005b. Modelling the sorption of Mn(II), Co(II), Ni(II), Zn (II), Cd(II), Eu(III), Am(III), Sn(IV), Th(IV), Np(V) and U(VI) on montmorillonite: Linear free energy relationships and estimates of surface binding constants for some selected heavy metals and actinides. Geochim. Cosmochim. Acta 69, 875–892. https://doi.org/10.1016/j.gca.2004.07.020.

Bradbury, M.H., Baeyens, B., 2009a. Sorption modelling on illite part I: titration measurements and the sorption of Ni, Co, Eu and Sn. Geochim. Cosmochim. Acta 73, 990–1003. https://doi.org/10.1016/j.gca.2008.11.017.

Bradbury, M.H., Baeyens, B., 2009b. Sorption modelling on illite. Part II: actinide sorption and linear free energy relationships. Geochim. Cosmochim. Acta 73, 1004–1013. https://doi.org/10.1016/j.gca.2008.11.016.

Charlton, S.R., Parkhurst, D.L., 2011. Modules based on the geochemical model PHREEQC for use in scripting and programming languages. Comput. Geosci. 37, 1653–1663. https://doi.org/10.1016/j.cageo.2011.02.005.

Clark, S.J., Segall, M.D., Pickard, C.J., Hasnip, P.J., Probert, M.I.J., Refson, K., Payne, M.C., 2009. First principles methods using CASTEP. Zeitschrift für Kristallographie - Crystalline Materials 220, 567–570. https://doi.org/10.1524/zkri.220.5.567.65075.

Dähn, R., Baeyens, B., Bradbury, M.H., 2011. Investigation of the different binding edge sites for Zn on montmorillonite using P-EXAFS – the strong/weak site concept in the 2SPNE SC/CE sorption model. Geochim. Cosmochim. Acta 75, 5154–5168. https://doi.org/10.1016/j.gca.2011.06.025.

De Cannière, P., Maes, A., Williams, S., Bruggeman, C., Beauwens, T., Maes, N., Cowper, M., 2010. Behaviour of Selenium in Boom Clay. (SCK•CEN-ER-120).

Ervanne, H., Puukko, E., Hakanen, M., 2013. Modeling of Sorption of Eu, Mo, Nb, Ni, pa, se, Sn, Th and U on Kaolinite and Illite in Olkiluoto Groundwater Simulants. Laboratory of Radiochemistry, Department of Chemistry, University of Helsinki.

Ervanne, H., Hakanen, M., Lehto, J., 2016. Selenium sorption on clays in synthetic groundwaters representing crystalline bedrock conditions. J. Radioanal. Nucl. Chem. 307, 1365–1373. https://doi.org/10.1007/s10967-015-4254-7.

Ewing, R.C., 2015. Long-term storage of spent nuclear fuel. Nat. Mater. 14, 252–257.

Gaines, G.L., Thomas, H.C., 1953. Adsorption studies on clay minerals. II. A formulation of the thermodynamics of exchange adsorption. J. Chem. Phys. 21, 714–718. https://doi.org/10.1063/1.1698996.

Gilbert, M., Laudelout, H., 1965. Exchage properties of hydrogen ions in clays. Soil Sci. 100, 157–162.

Hoehn, E., Eikenberg, J., Fierz, T., Drost, W., Reichlmayr, E., 1998. The Grimsel Migration Experiment: field injection–withdrawal experiments in fractured rock with sorbing tracers. J. Contam. Hydrol. 34, 85–106.

Ikonen, J., Sardini, P., Jokelainen, L., Siitari-Kauppi, M., Martin, A., Eikenberg, J., 2016a. The tritiated water and iodine migration in situ in Grimsel granodiorite. Part I: determination of the diffusion profiles. J. Radioanal. Nucl. Chem. 310, 1041–1048. https://doi.org/10.1007/s10967-016-4890-6.

Ikonen, J., Voutilainen, M., Söderlund, M., Jokelainen, L., Siitari-Kauppi, M., Martin, A., 2016b. Sorption and diffusion of selenium oxyanions in granitic rock. J. Contam. Hydrol. 192, 203–211. https://doi.org/10.1016/j.jconhyd.2016.08.003.

Jokelainen, L., Meski, T., Lindberg, A., Soler, J.M., Siitari-Kauppi, M., Martin, A., Eikenberg, J., 2013. The determination of 134Cs and 22Na diffusion profiles in granodiorite using gamma spectroscopy. J. Radioanal. Nucl. Chem. 295, 2153–2161. https://doi.org/10.1007/s10967-012-2268-y.

Kim, S.S., Min, J.H., Lee, J.K., Baik, M.H., Choi, J.W., Shin, H.S., 2012. Effects of pH and anions on the sorption of selenium ions onto magnetite. J. Environ. Radioact. 104, 1–6. https://doi.org/10.1016/j.jenvrad.2011.09.013.

Kitamura, A., Yamamoto, T., Nishikawa, S., Moriyama, H., 1999. Sorption behavior of Am (III) onto granite. J. Radioanal. Nucl. Chem. 239, 449–453. https://doi.org/10.1007/BF02349049.

Leach, A.R., 2001. Molecular Modelling: Principles and Applications, 2nd ed. Pearson Education.

Lehto, J., Hou, X., 2011. Chemistry and Analysis of Radionuclides Laboratory Techiques and Methodology. WILEY-VCH.

Li, X., Puhakka, E., Ikonen, J., Söderlund, M., Lindberg, A., Holgersson, S., Martin, A., Siitari-Kauppi, M., 2018. Sorption of Se species on mineral surfaces, part I: batch sorption and multi-site modelling. Appl. Geochem. 95, 147–157. https://doi.org/10.1016/j.apgeochem.2018.05.024.

Liu, S., Jacques, D., Govaerts, J., Wang, L., 2014. Conceptual model analysis of interaction at a concrete–boom clay interface. In: Physics and Chemistry of the Earth, Parts a/B/C, Mechanisms and Modelling of Waste-Cement and Cement-Host Rock Interactions. vols. 70–71. pp. 150–159. https://doi.org/10.1016/j.pce.2013.11.009.

Mahmoudzadeh, B., Liu, L., Moreno, L., Neretnieks, I., 2014. Solute transport in a single fracture involving an arbitrary length decay chain with rock matrix comprising different geological layers. J. Contam. Hydrol. 164, 59–71. https://doi.org/10.1016/j.jconhyd.2014.05.011.

Meng, S., Liu, L., Mahmoudzadeh, B., Neretnieks, I., Moreno, L., 2018. Solute transport along a single fracture with a finite extent of matrix: a new simple solution and temporal moment analysis. J. Hydrol. 562, 290–304. https://doi.org/10.1016/j.jhydrol.2018.05.016.

Missana, T., Alonso, Ú., García-Gutiérrez, M., Mingarro, M., 2008. Role of bentonite colloids on europium and plutonium migration in a granite fracture. Appl. Geochem. 23, 1484–1497. https://doi.org/10.1016/j.apgeochem.2008.01.008.

Missana, T., Alonso, U., Garcia-Gutierrez, M., 2009. Experimental study and modelling of selenite sorption onto illite and smectite clays. J. Colloid Interface Sci. 334, 132–138. https://doi.org/10.1016/j.jcis.2009.02.059.

Muuri, E., Ikonen, J., Matara-aho, M., Lindberg, A., Holgersson, S., Voutilainen, M., Siitari-Kauppi, M., Martin, A., 2016. Behavior of Cs in Grimsel granodiorite: sorption on main minerals and crushed rock. Radiochim. Acta 104, 575–582. https://doi.org/10.1515/ract-2016-2574.

Muuri, E., Siitari-Kauppi, M., Matara-aho, M., Ikonen, J., Lindberg, A., Qian, L., Koskinen, L., 2017. Cesium sorption and diffusion on crystalline rock: Olkiluoto case study. J. Radioanal. Nucl. Chem. 311, 439–446. https://doi.org/10.1007/s10967-016-5087-8.

Muuri, E., Sorokina, T., García, D., Grivé, M., Bruno, J., Koskinen, L., Martin, A., Siitari-Kauppi, M., 2018. The in-diffusion of 133Ba in granitic rock cubes from the Olkiluoto and Grimsel in-situ test sites. Appl. Geochem. 92, 188–195. https://doi.org/10.1016/j.apgeochem.2018.03.011.

Posiva Oy, 2013. Safety Case for the Disposal of Spent Nuclear Fuel at Olkiluoto. Models and Data for the Repository System 2012. Parts 1 and 2. Posiva Oy (POSIVA Report 2013-1).

Puhakka, E., Olin, M., 2014. Ab initio studies on cation exchange and surface complexation reactions on biotite surface, in: Final Workshop Proceedings of the Collaborative Project "Crystalline ROCK Retention Processes" (7th EC FP CP CROCK), KIT Scientific Report 7656, KIT Scientific Publishing, Karlsruhe. pp. 125–131. http://dx.doi.org/https://doi.org/10.5445/KSP/1000037468.

Puhakka, E., Li, X., Ikonen, J., Siitari-Kauppi, M., 2017. Sorption of Selenium Species onto Biotite and Calcite Surfaces: DFT Study. Migration 2017 Conference Poster.

Rovira, M., Gimenez, J., Martinez, M., Martinez-Llado, X., de Pablo, J., Marti, V., Duro, L., 2008. Sorption of selenium(IV) and selenium(VI) onto natural iron oxides: goethite and hematite. J. Hazard. Mater. 150, 279–284. https://doi.org/10.1016/j.jhazmat.2007.04.098.

Schulthess, C.P., Sparks, D.L., 1986. Backtitration technique for proton isotherm modeling of oxide surfaces. Soil Sci. Soc. Am. J. 50, 1406. https://doi.org/10.2136/sssaj1986.03615995005000060007x.

Shahkarami, P., Liu, L., Moreno, L., Neretnieks, I., 2016. The effect of stagnant water zones on retarding radionuclide transport in fractured rocks: an extension to the Channel Network Model. J. Hydrol. 540, 1122–1135. https://doi.org/10.1016/j.jhydrol.2016.07.031.

SKB, 1999a. Deep Repository for Spent Nuclear Fuel SR 97 - Post-Closure Safety Main Report. Technical Report TR-99-06 Volume I.

SKB, 1999b. Deep repository for spent nuclear fuel SR 97 - post-closure safety main report volume II. In: Technical Report TR-99-06.

Söderlund, M., Hakanen, M., Lehto, J., 2016a. Sorption of cesium on boreal forest soil I: the effect of grain size, organic matter and mineralogy. J. Radioanal. Nucl. Chem. 309, 637–645. https://doi.org/10.1007/s10967-015-4612-5.

Söderlund, M., Virkanen, J., Holgersson, S., Lehto, J., 2016b. Sorption and speciation of selenium in boreal forest soil. J. Environ. Radioact. 164, 220–231. https://doi.org/10.1016/j.jenvrad.2016.08.006.

Söderlund, M.J., 2016. Sorption and Speciation of Radionuclides in Boreal Forest Soil (Doctoral thesis). University of Helsinki, Finland.

Soler, J.M., Mäder, U.K., 2007. Mineralogical alteration and associated permeability changes induced by a high-pH plume: Modeling of a granite core infiltration experiment. Appl. Geochem. 22, 17–29. https://doi.org/10.1016/j.apgeochem.2006.07.015.

Soler, J.M., Landa, J., Havlova, V., Tachi, Y., Ebina, T., Sardini, P., Siitari-Kauppi, M., Eikenberg, J., Martin, A.J., 2015. Comparative modeling of an in situ diffusion experiment in granite at the Grimsel Test Site. J. Contam. Hydrol. 179, 89–101. https://doi.org/10.1016/j.jconhyd.2015.06.002.

Tachi, Y., Ebina, T., Takeda, C., Saito, T., Takahashi, H., Ohuchi, Y., Martin, A.J., 2015. Matrix diffusion and sorption of Cs+, Na+, I– and HTO in granodiorite: Laboratory-scale results and their extrapolation to the in situ condition. J. Contam. Hydrol. 179, 10–24. https://doi.org/10.1016/j.jconhyd.2015.05.003.

Tsai, S.C., Wang, T.H., Li, M.H., Wei, Y.Y., Teng, S.P., 2009. Cesium adsorption and distribution onto crushed granite under different physicochemical conditions. J. Hazard. Mater. 161, 854–861. https://doi.org/10.1016/j.jhazmat.2008.04.044.

Vilks, P., Cramer, J.J., Jensen, M., Miller, N.H., Miller, H.G., Stanchell, F.W., 2003. In situ diffusion experiment in granite: phase I. J. Contam. Hydrol. 61, 191–202. https://doi.org/10.1016/s0169-7722(02)00135-3.

Wang, P., Anderko, A., Turner, D.R., 2001. Thermodynamic modeling of the adsorption of radionuclides on selected minerals. II:anions. Ind. Eng. Chem. Res. 40, 4444–4455. https://doi.org/10.1021/ie000992h.

Widestrand, H., Byegård, J., Cvetkovic, V., Tullborg, E.L., Winberg, A., Andersson, P., Siitari-Kauppi, M., 2007. Sorbing tracer experiments in a crystalline rock fracture at Äspö (Sweden): 1. Experimental setup and microscale characterization of retention properties. Water Resour. Res. 43, W10413. https://doi.org/10.1029/2006wr005277.

Widestrand, H., Byegård, J., Nilsson, K., Höglund, S., Gustafsson, E., 2010. Long Term Sorption Diffusion Experiment (LTDE-SD) Performance of Main In Situ Experiment and Results from Water Phase Measurements. (SKB R-10-67).

Wissmeier, L., Barry, D.A., 2011. Simulation tool for variably saturated flow with comprehensive geochemical reactions in two- and three-dimensional domains. Environ. Model Softw. 26, 210–218. https://doi.org/10.1016/j.envsoft.2010.07.005.

Yang, X., Ge, X., He, J., Wang, C., Qi, L., Wang, X., Liu, C., 2018. Effects of mineral compositions on matrix diffusion and sorption of 75Se(IV) in granite. Environmental Science & Technology 52, 1320–1329. https://doi.org/10.1021/acs.est.7b05795.

Zheng, Z., Tokunaga, T.K., Wan, J., 2003. Influence of calcium carbonate on U(VI) sorption to soils. Environ. Sci. Technol. 37, 5603–5608. https://doi.org/10.1021/es0304897.